Journal of Colloid and Interface Science 626 (2022) 824–835

Contents lists available at ScienceDirect

Journal of Colloid and Interface Science

journal homepage: www.elsevier.com/locate/jcis

Effect of interparticle forces on the stability and droplet diameter of Pickering emulsions stabilized by PEG-coated silica nanoparticles

Daniel Hatchell *, Wen Song, Hugh Daigle

Hildebrand Department of Petroleum and Geosystems Engineering, University of Texas at Austin, USA

GRAPHICAL ABSTRACT

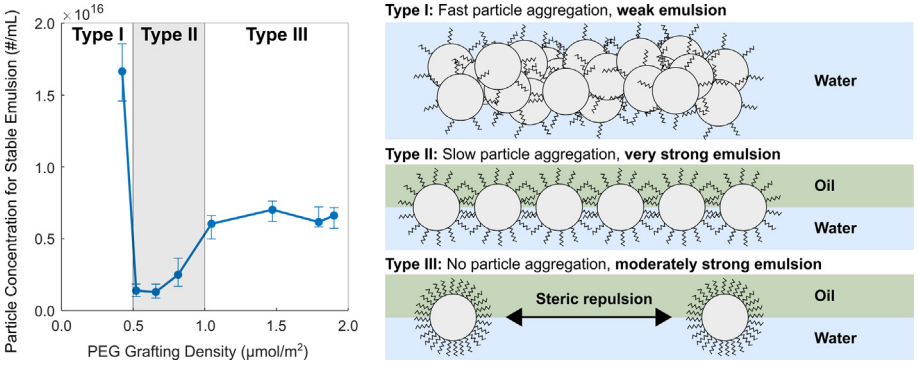

ARTICLE INFO

Article history:
Received 28 March 2022
Revised 13 June 2022
Accepted 1 July 2022
Available online 5 July 2022

Keywords:
Nanoparticles
Pickering emulsions
DLVO
Centrifugation
Microscopy

ABSTRACT

Hypothesis: Attractive and repulsive interparticle forces influence the stability and structure of Pickering emulsions. The effect these forces have on emulsion behavior must be better understood to improve Pickering emulsions for subsurface applications, including enhanced oil recovery and aquifer decontamination. Past work demonstrates improved emulsion stability with increasing salinity and reduced electrostatic repulsion, possibly because of interparticle networks. We hypothesize that emulsion stability is similarly improved by reducing interparticle steric repulsion.

Experiments: We assessed the effect of interparticle forces on emulsion stability by generating decane-in-water emulsions. We used polyethylene glycol (PEG)-coated silica nanoparticles with different diameters, surface modification, and salinities to modify either vdW, steric, or electrostatic interactions. We measured emulsion stability using centrifugation, imaged emulsion droplets with optical microscopy, and analyzed images with ImageJ to calculate droplet diameters.

Findings: Mildly aggregated particles with 0.5–1.0 μmol/m^2 surface PEG exhibit the highest emulsion stability. This optimal surface concentration maximizes a trade-off between particle repulsion and aggregation. Droplet diameters are well explained by an energy balance limited coalescence model, generated by solving DLVO equations. We find that while emulsion stability is influenced by interparticle forces, droplet size is dominated by particle-droplet interactions. These results demonstrate the potential of surface modification to significantly improve emulsion stability.

* Corresponding author at: 200 E Dean Keeton Street, Stop C0300, Austin, TX 78712-1585, USA.
E-mail address: dchatchell@utexas.edu (D. Hatchell).

https://doi.org/10.1016/j.jcis.2022.07.004
0021-9797/

1. Introduction

Nanoparticle-stabilized emulsions (i.e., Pickering emulsions) are a particularly stable form of emulsification and are used broadly [1–6], including the petroleum industry (in particular, for enhanced oil recovery and aquifer decontamination) [7–11], food science [12,13], biomedicine [14,15], and other fields [16,17]. Nanoparticles stabilize Pickering emulsions by partitioning to the fluid-fluid interface and physically blocking droplet coalescence [18,19]. This mechanism contrasts with more conventional surfactants that stabilize emulsions by reducing interfacial tension between fluids. The position of solid particles at a Pickering interface is favorable because the particle occupies an area that previously separated two immiscible fluids. The change in energy after particle attachment (the attachment energy, ΔE) is expressed as [1]:

$$\Delta E = \pi r^2 \gamma (1 - |cos(\theta)|)^2 \quad (1)$$

where r is the particle radius, γ is the fluid–fluid interfacial tension, and θ is the contact angle between the two fluids at the solid particle surface, measured from the wetting phase. The potential for high attachment energies and consequently high emulsion stability make nanoparticles attractive alternatives or additives to surfactants as emulsifying agents, especially in extreme conditions (high temperature, pressure, and salinity) [20].

The structure and stability of Pickering emulsions appear to be influenced strongly by particle interactions, although the specifics of these effects are unclear. Several studies observed that mild particle aggregation can improve emulsion stability greatly [21–25]. This phenomenon is thought to be caused by interparticle networks [26–28], a process where interacting particles arrange into rigid three-dimensional networks between emulsion droplets that increase the emulsion's resistance to creaming and coalescence. The specific conditions that lead to interparticle networks and optimal emulsion stability are not fully understood. There is a demand for very stable Pickering emulsions at low particle concentrations, especially in subsurface applications such as enhanced oil recovery and aquifer contamination. Further study of this behavior is needed to develop new approaches that increase emulsion stability.

Building from the original DLVO theory [29,30], interactions of nanoparticles in the bulk (i.e., unattached) and at the droplet interface (i.e., attached) can be described in terms of an extended DLVO theory [31–33]. Under the extended DLVO theory, the total interactions between two particles arise from the van der Waals (i.e., vdW), electrostatic, and steric forces. The vdW force is a short-range attractive force caused by the sum of interactions driven by fluctuations in electron density between nearby atoms within the two particles. Electrostatic forces act to repel particles with electrical charges of the same sign. The steric force is a repulsive force caused by overlapping electron clouds of atoms on particle surfaces when two particles approach. Altogether, the total interaction potential, Φ_T, is equal to the sum of the energies associated with these three forces, given below:

$$\Phi_T = \Phi_{vdW} + \Phi_E + \Phi_s. \quad (2)$$

Φ_{vdW}, Φ_E, and Φ_S refer to the vdW, electrostatic, and steric interaction energies, respectively. A small or negative Φ_T between particles is a predictor for particle aggregation; similarly, particles with large, positive Φ_T are expected to be stable.

The effect of electrostatic interactions on emulsion behavior is well documented in the literature. There is substantial experimental evidence that Pickering emulsion stability increases with increasing aqueous phase salinity [34–41]. As salinity increases, the electrostatic field is screened by free ions in the aqueous phase, the Debye length decreases, and Φ_E trends towards zero [34]. As a result, particles flocculate more easily and can produce very stable emulsions [41]. This effect is observed in emulsions with oil–water ratios less than 0.5 [35,37,40], although it appears to be most significant at oil–water ratios of 0.5 or higher [34]. The effects of steric and vdW interactions on emulsion behavior, however, are less clear. Raghavan et al. demonstrated that colloidal interactions between dispersed particles are varied with steric effects by replacing Si-OH groups at the particle surface with non-polar alkyl ligands [42]. Others have shown that steric interactions are altered by surface modifications that induce particle aggregation [43], optimize particle targeting [44], and stabilize uncharged surfactant-stabilized emulsion droplets [45]. While vdW attraction is known to cause particle aggregation in the absence of electrostatic and steric repulsion, it is difficult to manipulate vdW forces in a controlled setting. Studies on the effect of particle diameter on emulsion properties show that larger particles lead to larger, less-stable emulsion droplets, holding particle concentration equal [46–48]. From the Derjaguin approximation, attractive vdW forces are expected to increase with increasing nanoparticle diameter [49].

This work examines the effects of steric repulsion on the formation and stability of Pickering emulsions. We hypothesize that interparticle networks can be induced by controlling Φ_S, similar to research demonstrating improved emulsion stability in high salinity conditions with low Φ_E, thought to be driven by the formation of interparticle networks. First, to measure the importance of steric forces, we grafted silica nanoparticles with 3-[methoxy(polyethyleneoxy)6-9]propyltrimethoxysilane (PEG-silane) and adjusted the grafted surface density to manipulate Φ_S (holding Φ_{vdW} and Φ_E constant). Using centrifugation to measure emulsion stability, we discovered and quantified an intermediate grafting density that maximized interparticle networks while preventing excessive particle aggregation. Second, attempting to measure the influence of vdW forces, we generated Pickering emulsions that kept Φ_S constant while varying Φ_E, and investigated if changes in Φ_{vdW} via different particle diameters affect emulsion stability. Finally, we combined all three DLVO interactions into an energy balance model to calculate emulsion droplet diameter, agreeing with our experimental microscopy data. Our results help explain emulsion stability in terms of interparticle DLVO interactions, but show that emulsion droplet diameter is dominated by particle-droplet interactions. Further, we observe large increases in emulsion stability with careful control of Φ_S, introducing a new consideration of particle design to generate stable Pickering emulsions at low particle concentrations.

2. Materials and methods

2.1. Materials

NexSil 6, 12, and 20 silica nanoparticles (CAS: 7631-86-9; Lot No. 112820, 110178, and 105704; Nyacol) with average diameters of 6, 12, and 20 nm, respectively, were used as the bare nanoparticles for polymer grafting. Here, the particles are referred to by their diameter, with properties given in Table S1.

The particles are spherical amorphous silica stabilized in a basic aqueous solution. We used 3-[methoxy(polyethyleneoxy)6-9]propyltrimethoxysilane (PEG-silane, CAS: 65994-07-2, >99% purity, Gelest) to graft PEG ligands to the silica surface. *n*-decane (CAS: 124-18-5, >99% purity, Chevron Phillips) was used as the oil phase in all emulsions. Sodium chloride (NaCl, CAS: 7647-14-5, 99.5% purity, Fischer Scientific), calcium chloride ($CaCl_2$, CAS: 7440-70-2, 97% purity, Fischer Scientific), and deionized water (DIW) were used to make 5API brine (4 wt% NaCl, 1 wt% $CaCl_2$, 95 wt% DIW).

DIW was produced from a Barnstead E-Pure Ultrapure Water Purification System at 18.2 MΩ·cm.

2.2. Surface modification of silica nanoparticles with PEG-silane to produce PEG-NP

The reaction to graft PEG-silane to the silica surface followed a similar procedure to past work [32,50]. Stock nanoparticle solution containing 2 g of silica was mixed with DIW and PEG-silane in a vial at a combined mass of 20 g (10 wt% silica). The amount of PEG-silane added to the reaction was proportional to the desired PEG grafting density, and is described in more detail in Section 3.1. The vial was sealed with PTFE tape and stirred overnight above 65 °C to hydrolyze and condense the PEG-silane to the silica surface.

Following the reaction, the particle dispersion was pipetted into an Amicon Ultra-15 30 k MWCO centrifuge filter and washed with DIW eight times for 30 min at 5000 g. The retentate from the final wash was sonicated in DIW to disperse the clean particles. We refer to the final sonicated product as PEG-NP. Three samples from each batch of PEG-NP produced were extracted, weighed, and heated in an oven for 3 h at 120 °C to remove water and calculate an average nanoparticle mass concentration (wt%) of the entire batch. We used this reaction and filtration procedure to produce 6 nm, 12 nm, and 20 nm particles with various PEG grafting densities.

2.3. Measurement of PEG surface density with thermogravimetric analysis (TGA)

PEG grafting density was measured using thermogravimetric analysis (TGA). We followed a method similar to past studies [28,32,41]. A sample of containing 5–10 mg of PEG-NP was dried overnight in an aluminum oxide crucible at 80 °C. The dried sample and crucible were placed in a Mettler Thermogravimetric Analyzer TGA/DSC 1. Under 50 mL/min of nitrogen (N_2, CAS: 7727–37-9, >99.99% purity, Praxair) flow, temperature was increased from 30 °C to 110 °C at a rate of 10 °C/min and held at 110 °C for 20 min to remove any remaining water. Temperature was then increased from 110 °C to 800 °C, and the change in mass was recorded. The organic fraction, f_o, was calculated as the fraction of mass lost during the transition from 110 °C to 800 °C with respect to the mass at the start of the transition. The PEG grafting density, φ_l, was calculated from f_o using Eq. (3):

$$\varphi_l = \frac{f_o - f_{o,np}}{(1 - f_o - f_i + f_{o,np}) S_A M_{TGA}}, \quad f_i = \frac{(f_o - f_{o,np}) M_{iTGA}}{M_{TGA}}. \tag{3}$$

Eq. (3) relates f_o with S_A, the specific surface area of the original silica particles, M_{TGA}, the molecular weight of the segment of PEG ligand removed at high temperature (404 g/mol), $f_{o,np}$, the apparent organic fraction measured from unmodified silica nanoparticles, and f_i, the inorganic mass fraction. The final term, f_i, represents mass from the PEG ligands that remain attached to the silica surface. We assume that the average molecular weight of the segment of PEG ligand that remains at high temperature, M_{iTGA}, is 52 g/mol.

2.4. Measurement of particle diameter and zeta potential

Particle diameters and zeta (ζ) potentials were measured using a Malvern Zetasizer Nano ZS. A 1 wt% sample of nanoparticles was prepared in either DIW or 5API brine. Particle diameters were measured in Malvern DTS 0012 cuvettes using dynamic light scattering and reported as the Z-average diameter; ζ potentials were measured in a Malvern DTS 1070 zetacell.

2.5. Measurement of particle three-phase contact angle

Particle contact angle was measured via the sessile drop method on a spin-coated glass surface. We prepared microscope slides by stirring them overnight with diluted 0.1 N hydrochloric acid (HCl, CAS: 7647-01-0, 12.1 N, Fischer Scientific) on a hot plate set to 70 °C. We further rinsed the surface with isopropanol (C_3H_8O, CAS: 67-63-0, >99.5% purity, MilliporeSigma) and DIW, and air-dried the slides. Once cleaned, we deposited enough 10 wt% aqueous nanoparticle solution to cover the glass surface and spin-coated the slide for 60 s at 1000 rpm (1000 rpm/s acceleration) in a Laurell WS-650-23 spin-coater.

The spin-coated slide was placed in an empty plastic container with flat edges, into which we pipetted decane as the continuous phase. With a pipette tip positioned above the spin-coated surface and below the decane-air interface, a 7.5 μL droplet of DIW or brine was deposited onto the glass and recorded at 7.6 FPS. The first frame of contact between the settled droplet and particle surface was analyzed by running sessile drop calculations in the OneAttension software from Biolin. Multiple measurements were taken for each batch of filtered particles and averaged into one data point for both DIW and brine.

2.6. Particle imaging with transmission electron microscopy (TEM)

Transmission electron microscopy (TEM) was carried out with a JEOL NEOARM electron microscope to visualize particle size distribution and morphology. The imaging was performed using aberration-corrected STEM at 80 kV. To prepare the particles for imaging, a 20 μL sample of dilute PEG-NP (0.1 to 1 wt%) was dropped onto a 300-mesh carbon-gold lacey grid. The grid and particles were heated to 100 °C for 30 min before imaging to mitigate carbon contamination. Imaging was conducted for 6, 12, and 20 nm PEG-NP, but not for ungrafted silica, which was unstable and flocculated when dried.

2.7. Emulsion generation

Emulsions were produced with tip sonication, following similar procedures to past work [41]. First, we prepared an aqueous dispersion of DIW or 5API brine containing PEG-NP with the desired diameter, PEG grafting density, and mass concentration in the aqueous phase. We then combined 20 mL of the aqueous dispersion with 20 mL of decane in a 50 mL glass beaker. Sonication was performed with a Branson 450 Digital Sonifier. A 5 mm microtip was positioned in the center of the beaker at the aqueous/oleic interface, and the sample was sonicated three times for 10 s at 50% amplitude. The sample was lightly stirred after each 10 s pulse. The final product was a fully emulsified oil-in-water mixture.

2.8. Centrifugation

Emulsion stability was evaluated with centrifugation, similar to previous studies [39,41]. 30 g of freshly sonicated emulsion was transferred to a Falcon 50 mL polypropylene conical centrifuge tube. The tube was then centrifuged for 15 min in an Eppendorf 5810R Centrifuge at 5000 g. Centrifuge forces caused the continuous aqueous phase to separate below the emulsion and caused any coalesced decane to separate above the emulsion. The separated decane was extracted with a pipette and the change in emulsion mass was recorded. Emulsion stability was quantified as the volume fraction of decane separated and extracted during this process, with larger volume fractions of decane being released in weaker emulsions, and smaller or negligible volume fractions separating in stronger emulsions.

2.9. Optical microscopy and droplet size calculation

To quantify emulsion size distributions, direct measurements were enabled using optical microscopy. Emulsions were diluted in the appropriate aqueous phase (DIW or 5API brine) to aid droplet visibility and pipetted onto a glass microscope slide with a cover slip. We used an optical microscope (Nikon Labophot-Pol) and Nikon Digital Sight DS-Fil camera to take at least 10 images for each emulsion at resolutions of 0.271 μm/pixel (40x magnification), 1.08 μm/pixel (10x magnification), and 2.71 μm/pixel (4x magnification). Over 3000 images were captured and analyzed in total. We binarized the images in ImageJ and ran a particle analyzer on the oil droplets to obtain a distribution of droplet diameters from each magnification. The droplet diameters were combined into a single distribution, proportional to their coverage on the microscope slide, from which we calculated the Sauter mean diameter, D_{32}, given in Eq. (4):

$$D_{32} = \frac{\sum_i^n D_i^3}{\sum_i^n D_i^2} \tag{4}$$

where D_i refers to the diameter of droplet i in a distribution of n droplets. For the purpose of this calculation, the cover slide height was determined by measurement of focal planes to be approximately 50 μm; larger droplets that were flattened by this restriction were converted by their apparent shape under the microscope into an equivalent sphere from which their diameter, D_i, was obtained.

3. Results and discussion

We investigated the effect of Φ_S and Φ_{vdW} on emulsion stability by generating two separate sets of nanoparticles. For the first set, we grafted 6 nm silica nanoparticles with varying amounts of PEG-silane. We expect similar Φ_{vdW} for the particles given their constant diameter, and different Φ_S as the PEG concentration increased. For the second set, we varied the Φ_{vdW} while keeping Φ_S constant by grafting equal amounts of PEG-silane to particles with different diameters.

We characterized both sets of PEG-NP, including long-term stability measurements of the first set dispersed in brine (to observe differences in steric stability) and TEM images of the second set (to observe differences in particle diameter and polydispersity). These results are reported in Sections 3.1 and 3.2. From these results, we separated our particles into three categories. Type I particles had low concentrations (0–0.5 μmol/m^2) of PEG grafted to the silica surface, low Φ_S, and consequently poor long-term stability in brine, aggregating in under one minute. Type II particles had moderate concentrations (0.5–1.0 μmol/m^2) of surface PEG, intermediate Φ_S, and intermediate long-term stability in brine, with aggregation on timescales ranging from minutes to months. Type III particles had high concentrations (above 1.0 μmol/m^2) of surface PEG, high Φ_S, and excellent long-term stability in brine, likely requiring longer than one year to aggregate. The first set of PEG-NP (variable Φ_S) consisted of all three types; the second set (variable Φ_{vdW}) contained only Type III particles.

In Section 3.3, with our first set of PEG-NP, we show that Type II particles produced the most stable emulsions. Type I and III particles produced weak and moderately stable emulsions, respectively. These results are explained by a trade-off between particle aggregation and repulsion. When introduced to 5API brine, Type I particles aggregate and settle at the bottom of the solution on the order of seconds. These aggregates do not disperse during sonication, and as a result do not transfer to the oil–water interface when emulsions are first formed. The resulting Type I emulsions are weak and coalesce quickly. Type III particles, on the other hand, likely do not interact strongly enough to benefit from the increased stability observed in mildly flocculated particles [21–25]. Type II particles have enough surface PEG and Φ_S to resist complete aggregation, but slowly aggregate and mildly interact, leading to very strong emulsions. These three particle types are illustrated by Fig. 1. The results for the second set of PEG-NP were less conclusive, and we discuss them in Section S.3 of the supplemental material.

In Section 3.4, to understand the effect of DLVO interactions on emulsion droplet size, we developed an energy balance model based on DLVO equations to predict droplet diameter. We closely matched our predictions with diameter measurements from microscope images. Using this model, we explain key trends of droplet diameter as a function of particle concentration, particle diameter, and aqueous phase salinity from the perspective of energy balance equations. We show that, by replicating limited coalescence with an energy balance, emulsion droplet size is controlled by particle-droplet interactions, and not by interparticle forces.

3.1. Nanoparticle characterization

We reacted silica nanoparticles in the presence of PEG-silane, ranging from 0.5 to 16 μmol of PEG-silane in the reaction per square meter of particle surface area. Fig. 2 plots the TGA-measured PEG grafting density for both sets of particles as a function of PEG-silane added to the reaction [51]. These measurements demonstrate that our reaction conditions are repeatable and capable of small changes in the PEG grafting density, allowing us to precisely control Φ_S. The reaction does not produce a significantly different result at different particle diameters.

Table S2 lists the PEG grafting density, Z-average particle diameter, ζ potential, and contact angle for each filtered batch of PEG-NP and stock NexSil particles [51]. The Z-average diameter decreased slightly from the original nanoparticle to the grafted PEG-NP for all particles. This decrease likely resulted from sonication after particle filtration, where aggregated particles were dispersed. Fig. 3 plots the (a) ζ potential and (b) three-phase particle-decane-water contact angle of the first set of PEG-NP (6 nm) as a function of the PEG grafting density. We observed a small decrease in the magnitude of ζ potential with increasing PEG grafting density, indicating that neutral PEG ligands replaced negatively charged hydroxyl groups at the silica surface (error bars represent the standard deviation of the zeta potential measurement). The ζ potential does not become positive because there are still several unreacted hydroxyl groups on the silica surface (7.6 μmol/m^2 of surface SiOH sites is often assumed). As described by the interaction potential isotherm, a decrease in the magnitude of ζ potential is associated with reduced hydrophilicity [52]. Correspondingly, as the PEG grafting density increased, we observed an increase in the three-phase contact angle with respect to the aqueous phase for both DIW and brine, indicating reduced hydrophilicity. There was no significant difference between the contact angles measured in DIW or brine. The shaded region represents two standard deviations of uncertainty in the coefficients of linear regression to the combined data.

The second set of PEG-NP (constant PEG grafting density of 1.65–1.85 μmol/m^2, varying particle diameter) was analyzed with TEM. Fig. 4 displays TEM images of the 6, 12, and 20 nm PEG-coated particles. Each image uses an identical scale for comparison. The particles were monodisperse, with some variance in diameter within each batch but no exceptionally large particles or aggregates present. Particle diameters were approximately consistent with their nominal sizes. These images demonstrate that the particles roughly correspond to spheres with predictable diameters and should be well represented by the extended DLVO equations.

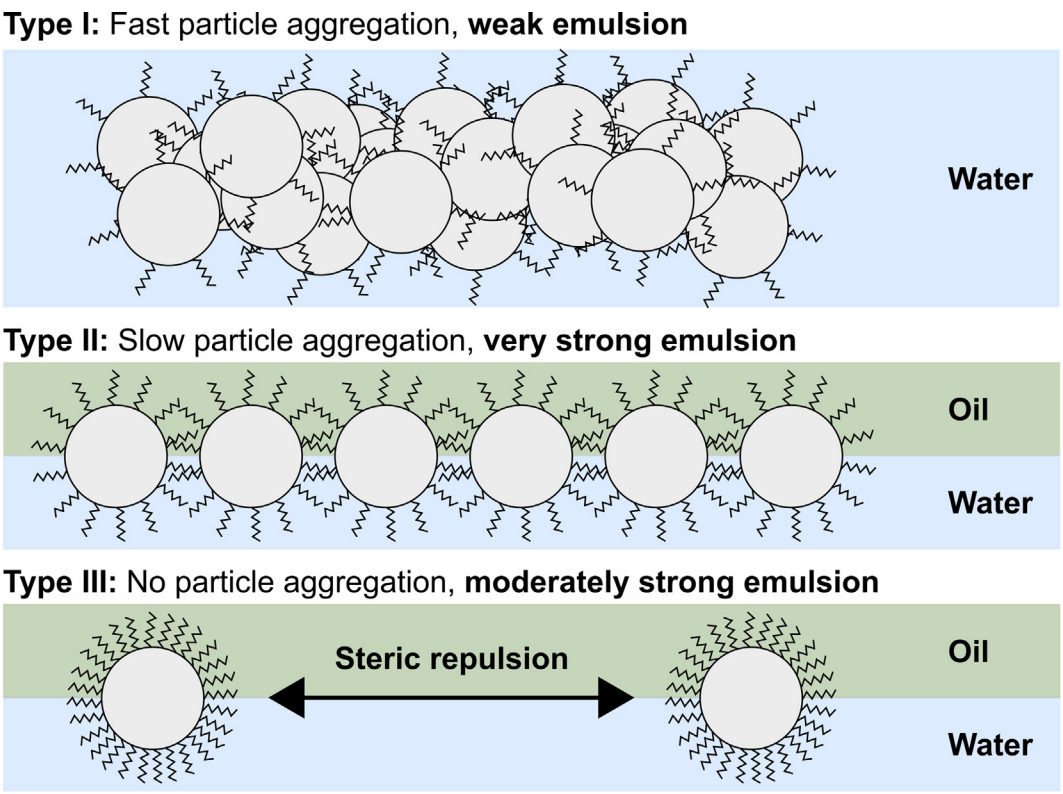

Fig. 1. Illustration of the effect of particle type on emulsion stability. Type I, II, and III particles refer to fast (<1 min), slow (days to months), and negligible (>1 year) aggregation rates, respectively. Type I particles interact too strongly and aggregate, leading to weak emulsions. Type II particles mildly flocculate and produce very strong emulsions. Type III particles are stable and brine and produce moderately strong emulsions; however, because they strongly repel each other with steric forces, they do not exhibit flocculation.

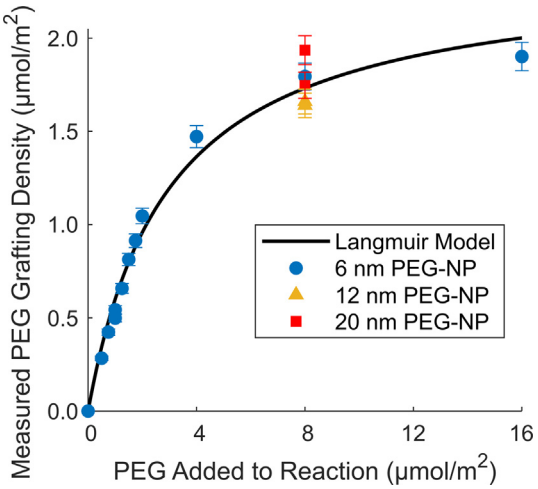

Fig. 2. PEG grafting density at the silica surface measured by TGA, plotted as a function of PEG-silane added to the reaction. The black line fits the data to a Langmuir adsorption model with a maximum coverage of 2.37 μmol/m^2.

3.2. Effect of PEG grafting density on the long-term stability of nanoparticles in brine

Before using our first set of PEG-NP (6 nm diameter, 0.28 μmol/m^2 to 1.90 μmol/m^2 PEG grafting density) to study the effect of Φ_S on emulsion behavior, we measured the long-term stability of the particles in 5API brine. We then compared the stabilities to DLVO calculations of the steric interaction to demonstrate that Φ_S was changing significantly with the PEG grafting density.

We mixed 1 wt% particles with 5API brine in a sealed vial and allowed them to sit at room temperature for six weeks, periodically measuring the DLS Z-average diameter of the samples and tracking the growth of particle size over time. Fig. 5 (a) plots the particle growth for different PEG grafting densities. The Z-average diameters ranged from 10 to 20 nm to 10000 nm, the upper limit of our measurement. The error bars for Z-average diameter represent two standard deviations, based on previous repeat measurements of similarly-sized particles. This error is approximately ± 10% of diameter for smaller particles and ± 40% for larger particles.

Particle stability to aggregation in 5API brine depended on the PEG grafting density. The particles with the smallest amount of PEG (0.28 μmol/m^2 PEG-NP, bare silica) aggregated immediately in brine and were not measured. PEG-NP with 0.42 μmol/m^2 PEG grafting density aggregated in less than one minute. As PEG grafting density increased, the timescale of aggregation increased by orders of magnitude, with.

0.52 μmol/m^2, 0.65 μmol/m^2, and 0.81 μmol/m^2 PEG-NP respectively taking a day, a week, and several months to aggregate. Above 1 μmol/m^2, aggregation was negligible over six weeks.

We calculated a stability ratio, W, to quantify the aggregation rate for each particle, using Eq. (5) [53]:

$$W = \frac{4k_B T N_o t_{1/2}}{3\mu} \tag{5}$$

where T is temperature, N_o is the initial number of nanoparticles present, $t_{1/2}$ is the half-life of particle aggregation, and μ is the viscosity of the continuous phase. The time for the number of nanoparticles to decrease by half, $t_{1/2}$, is determined by calculating the change in particle volume over time from the Z-average diameter.

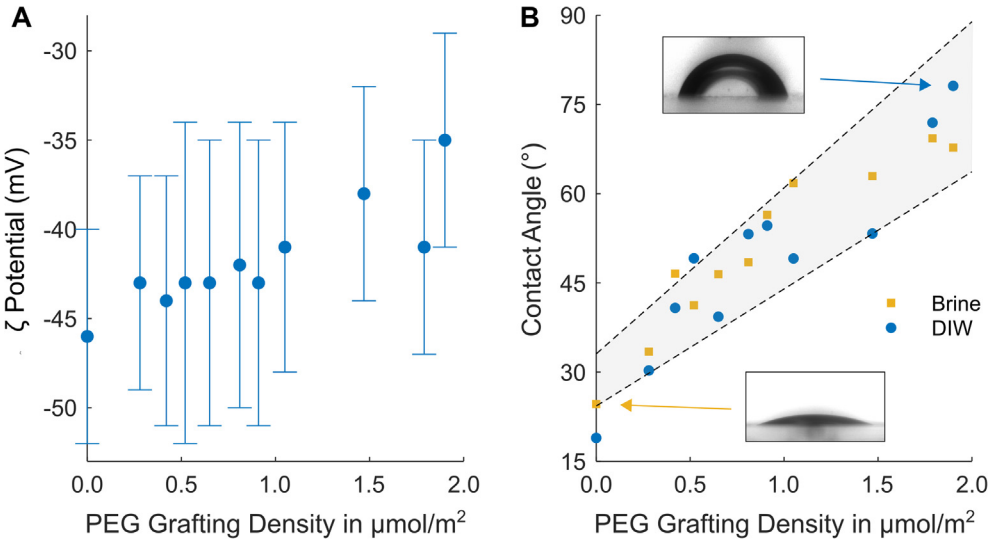

Fig. 3. (a) DLS-measured particle ζ potential in DIW as a function of PEG grafting density for 6 nm PEG-NP; (b) Particle-decane-water contact angle with respect to the aqueous phase (both DIW and brine) as a function of PEG grafting density for 6 nm PEG-NP. The two inset images show aqueous droplets on a spin-coated surface submerged in decane. Along with other measurements, they were analyzed with the sessile drop method to calculate the contact angle.

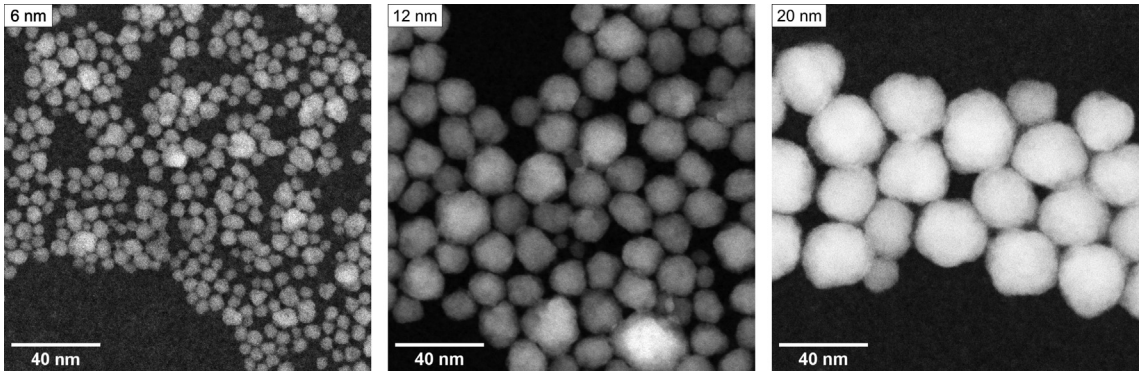

Fig. 4. TEM images of 6 nm, 12 nm, and 20 nm particles grafted with approximately 1.75 μmol/m^2 PEG surface density. Each image has an identical scale bar of 40 nm.

Fig. 5 (b) plots the stability ratio of each particle as a function of PEG grafting density. Error bars represent the slope error of an exponential fit to particle number versus time when calculating $t_{1/2}$. Below 0.5 μmol/m^2 PEG grafting density, particles aggregated too quickly to get an accurate measurement of W; we refer to the particles that aggregated in less than one minute as "Type I" and plot the upper limit of W (4×10^3) with an arrow indicating the direction of the true value. Between 0.5 μmol/m^2 and 1 μmol/m^2, particles exhibited aggregation timescales between one day and one year. We measured W values ranging from 2×10^6 to 1×10^9 for these particles with total error bars between ± 20% and ± 30% of W (large in the absolute sense, but small on a logarithmic scale). We categorized these particles as "Type II". Above 1 μmol/m^2, aggregation occurred too slowly to properly measure; we plot the minimum W (4×10^9) of these "Type III" particles with arrows indicating that the true W is likely far larger.

Fig. 5 (b) also plots the DLVO energy barrier of separation - the difference between DLVO local maximum and local minimum interaction energies (Φ_T) between two identical particles for different separation distances - as a function of PEG grafting density. The calculation of these interaction energy curves is described in detail in Section S.2 and Fig. S1 in the supplemental material (SM) [49,54,55]. As PEG grafting density increased, steric repulsion increased significantly, resulting in higher Φ_T. The DLVO energy barrier of separation follows the same general trend as the stability ratio, demonstrating that small amounts of PEG added to the particle surface greatly increased both steric repulsion and particle stability to aggregation.

3.3. Effect of DLVO interactions on emulsion stability

Using the results from nanoparticle characterization and long-term stability measurements, we verified that our first set of PEG-NP had varying PEG grafting density and Φ_S, while our second set of PEG-NP had different particle diameters, and as a result of the Derjaguin approximation [49], different Φ_{vdW}. With these properties confirmed, we could test the importance of each interaction on emulsion stability.

Our first goal was to use the first set of PEG-NP to determine the effect of Φ_S on emulsion stability. Using PEG grafting densities between 0.42 μmol/m^2 and 1.90 μmol/m^2, we generated decane-in-water emulsions with our 6 nm particles in 5API brine over a wide range of particle concentrations. The concentration range was chosen such that emulsions were completely stable to coalescence in the centrifuge on the high end of the range, and completely unstable to coalescence on the low end (with the understanding that increased particle concentration improved emulsion stability to centrifugation). Then, by centrifuging each

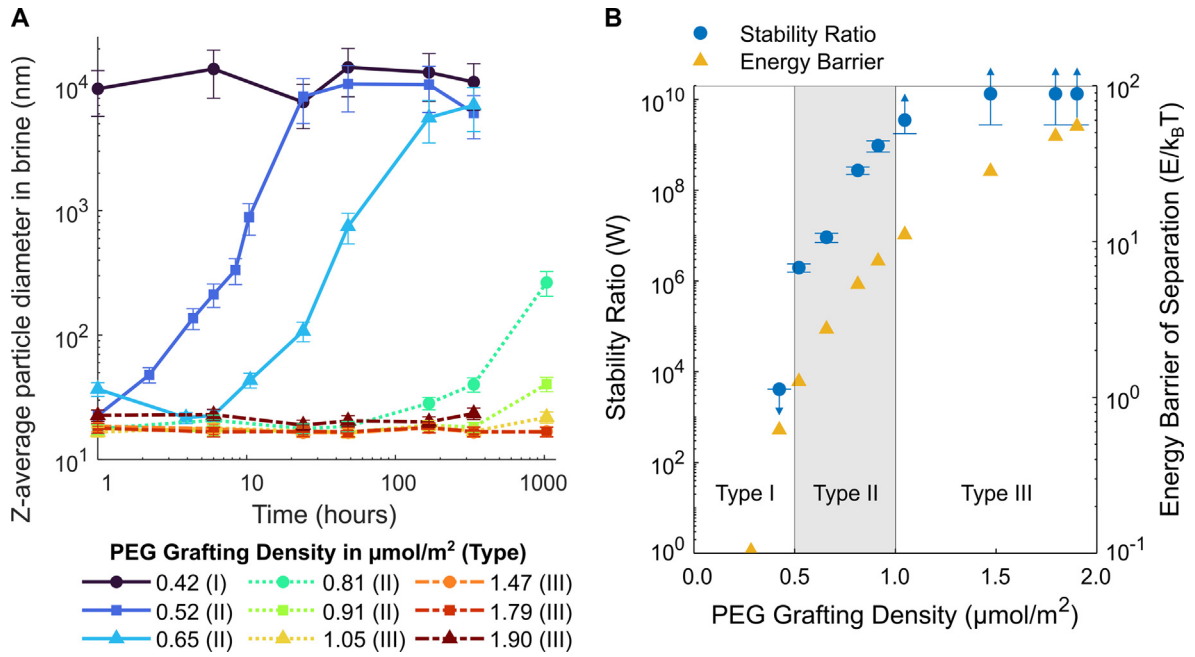

Fig. 5. (a) DLS-measured Z-average particle diameter in 5API brine over time, plotted for 6 nm, 0.42–1.90 μmol/m^2 PEG-NP. (b) Experimental stability ratio (W) and theoretical pairwise DLVO interaction potential energy barrier of 6 nm, 0.42–1.90 μmol/m^2 PEG-NP, plotted as a function of PEG grafting density. Arrows indicate that the measurement is limited by the timescale of aggregation, and the true value likely lies in the direction specified. Type I, II, and III particles refer to fast (<1 min), slow (days to months), and negligible (>1 year) aggregation rates, respectively.

emulsion across this concentration range, we identified the concentration of nanoparticles required to partially stabilize exactly 50% of the emulsion, and used this midpoint as a point of comparison. The results of this experiment are plotted in Fig. 6 (a) and summarized by the midpoint in Fig. 6 (b) [51].

Fig. 6 (a) displays stability curves for emulsions from each nanoparticle batch as a function of nanoparticle concentration. "Volume fraction of decane released" refers to the volume fraction of decane that separated out of the emulsion during centrifugation, and is a proxy for emulsion stability: less decane separated from stronger emulsions than from weaker emulsions because there were fewer droplet coalescence events. To account for small amounts of decane evaporating during sonication, if the measured volume fraction of separated decane was above 0.95, the volume fraction was set at 1. Error bars represent two standard deviations in the volume of decane released (approximately ± 9%), based on previous repeat measurements of comparable emulsions. Nanoparticle concentration refers to the number concentration of particles by volume of the aqueous phase, calculated by dividing the mass of particles in the emulsion by the mass of a single particle (estimated

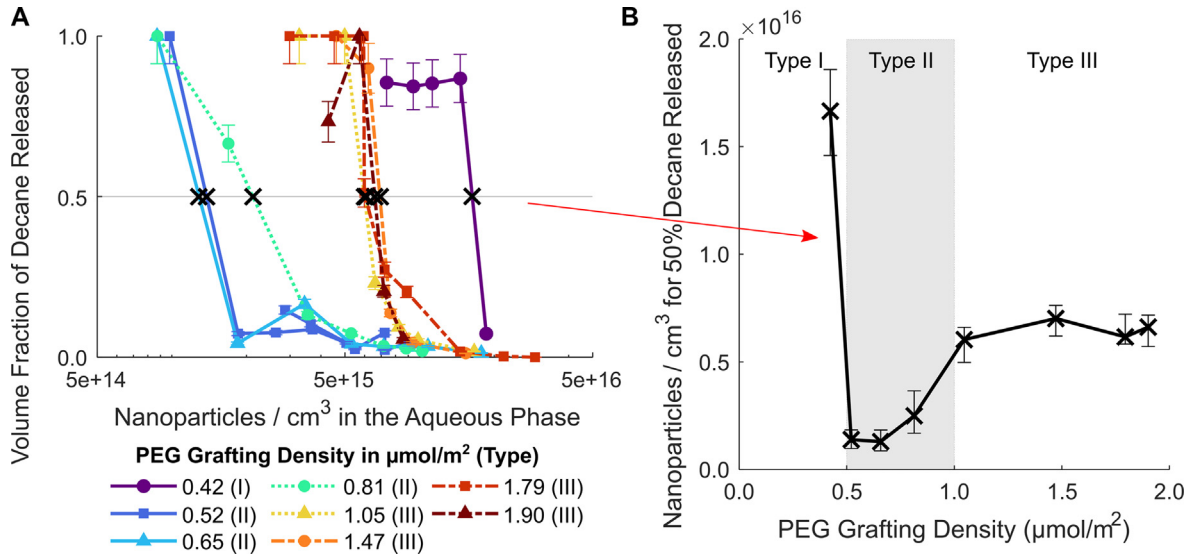

Fig. 6. (a) Volume fraction of decane released from decane-in-brine emulsions after centrifugation as a function of nanoparticle number concentration in the aqueous phase, plotted for 6 nm, 0.42–1.90 μmol/m^2 PEG-NP. (b) Nanoparticle number concentration in the aqueous phase required to produce an emulsion that releases 50% of its decane by volume after centrifugation, plotted as a function of PEG grafting density. This plot is constructed from the horizontal line drawn across (a). Type I, II, and III particles refer to fast (<1 min), slow (days to months), and negligible (>1 year, extrapolated from the data) aggregation rates, respectively.

using the volume and density of amorphous silica, as well as the added mass of PEG). We did not produce emulsions from the set of 0.91 μmol/m^2 PEG-NP.

Each particle transitioned from an unstable emulsion to a stable emulsion as particle concentration increased. To compare these particles, we took a horizontal slice of the data at 50% volume fraction of decane released and plotted the result in Fig. 6 (b), which shows the particle concentration required for 50% stability as a function of PEG grafting density. Error bars in Fig. 6 (b) represent the concentration of the nearest emulsions that released more than 60% or less than 40% of decane after centrifugation. The emulsions exhibited an interesting trend: at low PEG grafting densities (Type I particles), the emulsions were weak, with 0.42 μmol/m^2 PEG-NP requiring 1.7 × 10^{16} particles / cm^3 for 50% stability; 0.28 μmol/m^2 PEG-NP and bare silica failed to stabilize emulsions in brine at all. At moderate PEG grafting densities (Type II particles), the emulsions were very stable, requiring 1 to 3 × 10^{15} particles / cm^3 for 50% stability. Particles with higher PEG grafting densities (Type III particles) were less stable, needing 6–7 × 10^{15} particles / cm^3 to achieve the same stability.

If we only considered the interaction between a particle and the droplet interface, as described by Eq. (1), we would expect emulsion stability to increase monotonically with increasing PEG grafting density and consequently increased contact angle (as observed in Fig. 3 (b)). However, the trend from Fig. 6 (b) is better explained by coupling between steric repulsion and flocculation. Type I particles had low steric repulsion and likely aggregated too quickly in 5API brine to act as effective emulsifiers. As a result, the Type I emulsions were comparatively weaker. Type III particles, on the other hand, strongly resisted aggregation with high steric repulsion. The stability of Type III emulsions was higher than Type I emulsions. Type II emulsions were the strongest of the three; the Type II particles sufficiently resisted aggregation over the timescale required to generate an emulsion, but steric repulsion was low enough to allow for significant interparticle attraction, which is associated with high emulsion stability [21–25]. The improved emulsion stability was likely caused by interparticle networks [26–28], where electrostatic repulsion is sufficiently screened to allow particles to interact and flocculate partially. These findings are the first known quantification of a particle surface coverage that optimizes emulsion stability via changes in steric repulsion, and present a new approach for optimizing Pickering emulsion stability at low particle concentrations.

Our second goal was to evaluate the effect of Φ_{vdW} on emulsion stability. We repeated similar centrifugation experiments for our second set of PEG-NP, which are described in detail Section S.3 and Fig. S2. We found that smaller particles required a greater number concentration per volume of aqueous phase to stabilize an emulsion to the same extent as larger particles. We further observed that emulsions in DIW required a greater number concentration of particles to achieve the same stability as emulsions in 5API brine. This finding supports past work suggesting that reduced electrostatic repulsion in 5API brine promotes interparticle networks and increases emulsion stability [41]. Controlling for these two factors, we found that emulsions with 6 nm particles exhibited the smallest improvement in stability (1.5–2.4 times fewer nanoparticles) when switching from DIW to 5API brine, compared to emulsions with 12 nm (2.5–5.6 times fewer nanoparticles) or 20 nm particles (2.7–4.3 times fewer nanoparticles). This smaller improvement in stability with 6 nm particles may be evidence of smaller vdW attraction leading to weaker particle flocculation in brine, although the trend is unclear and needs additional study.

3.4. Effect of DLVO forces on droplet diameter

In addition to evaluating emulsion stability, we examined emulsion droplet diameter using microscopy. We took multiple microscope images at different magnifications from each emulsion presented in the previous sections and processed the images into a single representative measure of diameter, the Sauter diameter (D_{32}). Fig. 7 (a) through (e) plots D_{32} values as a function of nanoparticle mass concentration for different contexts: (a) varying particle diameter in brine, (b) varying particle diameter in DIW, (c) 6 nm PEG-NP in brine and DIW, (d) 12 nm PEG-NP in brine and DIW, and (e) 20 nm PEG-NP in brine and DIW. The solid and dashed lines are an energy balance model fit to the data, explained below. There was no significant trend in D_{32} for 6 nm particles with varying amounts of PEG grafting density, so those data points were combined into a single "6 nm, brine" curve in Fig. 7 (a) and (c). Fig. 7 (f), (g), and (h) represent emulsions generated particles with different characteristics (1 wt%, 6 nm, brine, D_{32} = 9.34 μm; 1 wt%, 12 nm, DIW, D_{32} = 45.9 μm; and 0.185 wt%, 20 nm, brine, D_{32} = 135 μm, respectively). These three emulsions are highlighted to demonstrate the range of particle properties and emulsion diameters observed under the microscope.

A few trends stand out from the D_{32} measurements. Emulsion droplets were larger in DIW than in 5API brine, holding particle diameter and concentration constant. Emulsion droplets also decreased in size with increasing particle concentration, and with decreasing particle diameter. Plots of D_{32} against particle concentration fit reasonably well to linear relations on a log–log scale. These observations agree with previous measurements [41], and are consistent with the particle-poor systems considered by limited coalescence models and experiments [56–58]. In limited coalescence models, the area occupied by an individual densely-packed nanoparticle forming part of an interfacial monolayer is multiplied by the number of particles at the droplet interface. The product is the total droplet surface area, and can be combined with the total volume of the dispersed phase to calculate an average droplet diameter. The number of particles at the droplet interface can range from 0 to 100% of the total. Salt ions in the aqueous phase act as a "promoter" and increase this percentage by suppressing electrostatic repulsion and assisting the transition of particles from the bulk to the droplet interface [56,57].

To determine the importance of interparticle forces on limited coalescence, we fitted a numerical energy balance model to the data based on DLVO interaction potentials at the oil–water interface. The energy balance model considers a starting condition of small decane droplets dispersed throughout the aqueous phase, analogous to assumptions made in emulsifier-poor limited coalescence models [56–58]. At the starting condition, all nanoparticles reside in the aqueous phase; no particles are present in the decane or at the brine-oil interface. We assume this starting condition is caused by sonication, where the oil phase is broken into a collection of small droplets. Without nanoparticles, these droplets coalesce rapidly (in a few seconds) into a continuous decane phase.

From the starting condition, we assume that a fraction of the particles transition from the aqueous phase to the brine-oil interface, until an energy equilibrium is achieved. The migration of particles to the interface in our model is governed by five energy terms: (1) vdW attraction between closely packed particles at the interface (Φ_{vdW}^{int}), which favors particle migration; (2) electrostatic repulsion between closely packed particles at the interface (Φ_{E}^{int}), which hinders particle migration; (3) steric repulsion between closely packed particles at the interface (Φ_{S}^{int}), which hinders particle migration; (4) reduced oil–water surface energy because of area

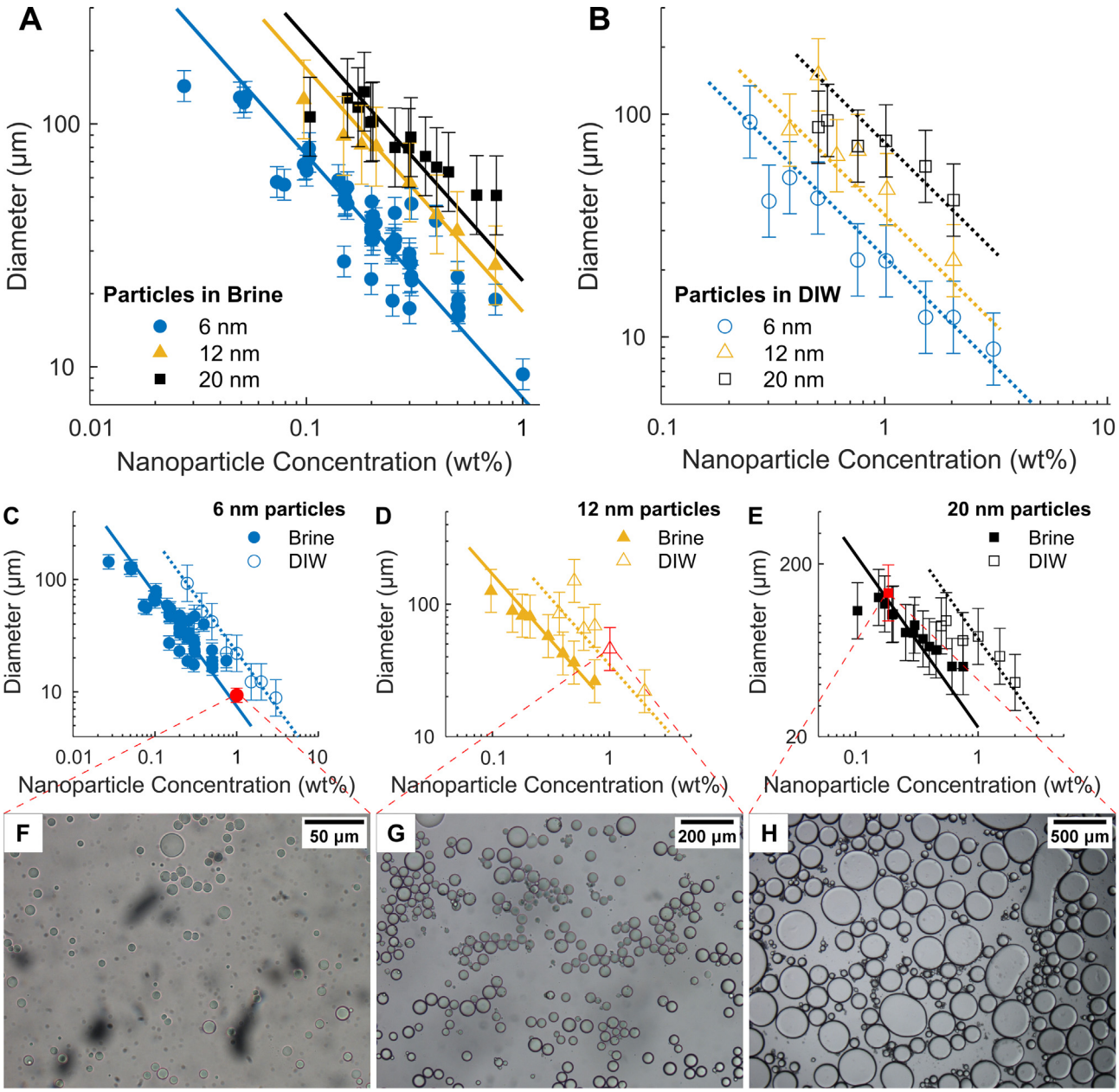

Fig. 7. Emulsion D_{32} diameter plotted as a function of nanoparticle concentration (wt%) and presented in the following contexts: (a) all brine emulsions plotted for different particle diameters; (b) all DIW emulsions plotted for different particle diameters; (c) all 6 nm PEG-NP plotted for brine and DIW; (d) all 12 nm PEG-NP plotted for brine and DIW; (e) all 20 nm PEG-NP plotted for brine and DIW. The solid or dashed lines demonstrate the energy balance model fitted to the droplet diameters. Particles with different PEG grafting densities are combined in the above plots where applicable. Images (f), (g), and (h) show microscope images from the emulsions corresponding to the data points indicated in plots (c), (d), and (e). The images are chosen to represent different particle diameters, salinity, and droplet sizes.

occupied by the interfacial particle ($\Delta_{int}G$), which favors particle migration; and (5) energy associated with the entropic demixing and arrangement of particles from the aqueous phase to the interface ($\Delta_{demix}G$), which hinders particle migration. The total energy E_{Total} of bringing a particle from the aqueous phase to the interface can be described as the sum of these five terms, using Eq. (6):

$$E_{Total} = \Phi_{vdW}^{int} + \Phi_{E}^{int} + \Phi_{S}^{int} + \Delta_{int}G + \Delta_{demix}G \quad (6)$$

The derivation of these five energy terms, as well as specific parameters used in our calculations, are described by Eq. (S8) through Eq. (S21) in Section S.4 of the SM, based primarily on research by Aveyard et al. [59] and other past work [60–62]. In practice, Φ_{vdW}^{int} and Φ_{E}^{int} are often insignificant in the final summation; E_{total} is typically negative because of the large magnitude of $\Delta_{int}G$, and particles transition to the interface until there are no more particles to attach to the interface ($\Delta_{demix}G$ approaches infinity) or particles can no longer be packed into the surface area available by sonication (Φ_{S}^{int} approaches infinity). The two cases represent the particle-poor and particle-rich regimes, respectively, of limited coalescence models.

Once the equilibrium distribution between particles at the interface and in the aqueous phase has been determined, we consider the density of particles at the interface of our initial sonication-generated oil droplets. For particle-rich systems, the equilibrium density of particles at the interface already forms a dense monolayer. In particle-poor systems, we assume that limited coalescence occurs, in which the sparsely-coated droplets coalesce and increase in diameter until the adsorbed particles form a dense

monolayer [56–58]. The oil droplet diameter required to pack the equilibrium number of interfacial particles into dense monolayers, D_{model}, is the output of our model. A detailed list summarizing the specific steps involved in our model is presented in Section S.5 of the SM.

The solid and dashed lines in Fig. 7 (a) through (e) display the results of our model fitted to the data, with three fitting parameters: L, the ligand length; AF_{DIW}, the particle attachment fraction in DIW; and AF_{Brine}, the particle attachment fraction in brine. Based on the structure of PEG, L should be less than 4 nm. AF_{DIW} and AF_{Brine} represent the fraction of particles permitted to transition to the droplet interface by the model, and are introduced to explain the differences of DIW and brine emulsions, as described in previous work with the concept of salt "promoters" [56,57]. Particle radii are obtained from DLS measurements. The exact parameters used to generate the model are listed in Table S3.

We see good agreement between our energy balance model and the data. While the cases of DIW and brine were fitted separately using AF_{DIW} and AF_{Brine}, the differences in droplet diameters predicted by 6 nm, 12 nm, and 20 nm particles arise naturally from the model. Holding the particle concentration constant, larger particles have less available cross-sectional area to form a monolayer, and therefore can only stabilize larger droplets. We find that Φ_{vdW}^{int} and Φ_E^{int} are too small in proportion to $\Delta_{int}G$ to meaningfully affect emulsion droplet size, and can be neglected. As a result, our model simplifies to a geometric limited coalescence model with particle-poor (controlled by $\Delta_{demix}G$) and particle-rich (controlled by Φ_S^{int}) regimes. Given our low particle concentrations, all of our measurements exist inside the particle-poor regime. One consequence of this simplification is that the model is insensitive to changes in θ, explaining the lack of measurable trend of D_{32} as a function of PEG grafting density for 6 nm PEG-NP. The energy balance model demonstrates that – unlike emulsion stability, which is strongly affected by interparticle forces – droplet diameter appears to be dominated by particle-droplet interactions, with Φ_S^{int} and $\Delta_{demix}G$ functioning only as boundary conditions.

4. Conclusions

We created PEG-coated silica nanoparticles with varying particle diameters and PEG grafting densities. We hypothesized that, in a manner analogous to studies that show improved emulsion stability with increasing salinity by reducing electrostatic repulsion [34–41], we could improve emulsion stability by reducing steric repulsion.

By modifying the PEG grafting density of 6 nm nanoparticles, we generated Type I (0 to 0.5 μmol/m^2 PEG), Type II (0.5 to 1 μmol/m^2 PEG), and Type III (1 to 2 μmol/m^2 PEG) particles that aggregated in timescales of less than one minute, from one minute to one year, and several years, respectively. We found that Type II emulsions were the most stable in 5API brine, requiring 1–3 $\times$ 10^{15} particles / cm^3 to achieve 50% stability to centrifugation. Type III emulsions required 6–7 $\times$ 10^{15} particles / cm^3 to achieve the same stability, and were less stable than Type II emulsions, even though Type III particles have higher contact angles and attachment energies. This difference is explained by the reduced steric repulsion and improved interparticle attractions between Type II particles, likely leading to interparticle networks and improved emulsion stability. The relative instability of Type I particles made Type 1 emulsions far less stable or completely unstable with 5API brine. These results are consistent with past research showing that particle flocculation can be controlled by surface modification [42,43], and that particle flocculation can lead to emulsion stability [21–25]. To our knowledge, these findings represent the first quantification of an optimal intermediate surface grafting density that balances particle flocculation with Pickering emulsion stability. These results introduce a new strategy for designing particles to generate stable Pickering emulsions, especially at low particle concentrations. Future work will attempt to reproduce these results on different grafting chemicals to see how the optimal coverage changes as a function of ligand chemistry. We repeated these experiments using particles with different diameters in DIW and 5API brine to isolate the influence of vdW attraction; however, we did not see a conclusive trend of improved emulsion stability at higher particle diameters. More sensitive experiments will be required in the future to determine if increased vdW attraction can improve emulsion stability.

We finally measured droplet diameters of our emulsions and fit them with an energy balance model, achieving a close match to the data. These measurements demonstrate that droplet diameter tends to increase with increasing particle size and decreasing particle concentration, consistent with past work [41]. This work adapts interfacial DLVO equations described by past studies [59–62] to a large experimental dataset, and builds on past limited coalescence models [56–58] by taking the perspective of energy equilibrium. Altogether, these results demonstrate that emulsion stability can be greatly impacted by particle interactions, whereas droplet diameter is unaffected by changes in Φ_{vdW}^{int} and Φ_E^{int}, and is influenced by Φ_S^{int} only as a particle-rich boundary condition. Both conclusions are important for informing particle selection for applications.

CRediT authorship contribution statement

Daniel Hatchell: Conceptualization, Methodology, Validation, Formal analysis, Investigation, Writing – original draft, Visualization. **Wen Song:** Conceptualization, Methodology, Writing – review & editing. **Hugh Daigle:** Conceptualization, Methodology, Resources, Writing – review & editing, Supervision, Project administration, Funding acquisition.

Declaration of Competing Interest

The authors declare that they have no known competing financial interests or personal relationships that could have appeared to influence the work reported in this paper.

Acknowledgements

The authors would like to thank Dr. Hugo Celio and Dr. Raluca Gearba for their assistance with running experiments on DLS and TGA, as well as Dr. Karalee Jarvis for assisting with TEM measurements. This work was supported by assistance from Nyacol Nano Technologies, who supplied nanoparticles. This material is based upon work supported by the US National Science Foundation Graduate Research Fellowship Program under Grant No. (DGE-1610403). Any opinions, findings, and conclusions or recommendations expressed in this material are those of the authors and do not necessarily reflect the views of the National Science Foundation. This work was further supported by the Nanoparticles for Subsurface Engineering Industrial Affiliates Program (member companies Nissan Chemical of America, Baker Hughes, and Foundation CMG) at the University of Texas at Austin.

Appendix A. Supplementary material

Supplementary data to this article can be found online at https://doi.org/10.1016/j.jcis.2022.07.004.

References

[1] B.P. Binks, Particles as surfactants—similarities and differences, Curr. Opin. Colloid Interface Sci. 7 (1–2) (2002) 21–41.
[2] Y. Chevalier, M.A. Bolzinger, Emulsions stabilized with solid nanoparticles: Pickering emulsions, Colloids Surf., A 439 (2013) 23–34.
[3] J. Wu, G.H. Ma, Recent studies of Pickering emulsions: particles make the difference, Small 12 (34) (2016) 4633–4648.
[4] Y. Yang, Z. Fang, X. Chen, W. Zhang, Y. Xie, Y. Chen, W. Yuan, An overview of Pickering emulsions: solid-particle materials, classification, morphology, and applications, Front. Pharmacol. 8 (2017) 287.
[5] D. Arab, A. Kantzas, S.L. Bryant, Nanoparticle stabilized oil in water emulsions: A critical review, J. Petrol. Sci. Eng. 163 (2018) 217–242.
[6] L.E. Low, S.P. Siva, Y.K. Ho, E.S. Chan, B.T. Tey, Recent advances of characterization techniques for the formation, physical properties and stability of Pickering emulsion, Adv. Colloid Interface Sci. 277 (2020) 102–117.
[7] J.R. Bragg, U.S. Patent No. 5,855,243, U.S. Patent and Trademark Office, Washington, DC, 1999.
[8] R.D. Kaminsky, R.C. Wattenbarger, J. Lederhos, S.A. Leonardi, Viscous oil recovery using solids-stabilized emulsions, in: SPE Annual Technical Conference and Exhibition, Society of Petroleum Engineers, 2010, January.
[9] S. Ko, E.S. Kim, S. Park, H. Daigle, T.E. Milner, C. Huh, M.V. Bennetzen, G.A. Geremia, Amine functionalized magnetic nanoparticles for removal of oil droplets from produced water and accelerated magnetic separation, J. Nanopart. Res. 19 (4) (2017) 132.
[10] S. Ko, C. Huh, Use of nanoparticles for oil production applications, J. Petrol. Sci. Eng. 172 (2019) 97–114.
[11] J.X. Liu, H.J. Zhu, P. Wang, J.M. Pan, Recent studies of Pickering emulsion system in petroleum treatment: The role of particles, Pet. Sci. 18 (5) (2021) 1551–1563.
[12] B.S. Murray, Pickering emulsions for food and drinks, Curr. Opin. Food Sci. 27 (2019) 57–63.
[13] J. Weiss, T. Ahmad, C. Zhang, H. Zhang, A review of recent progress on high internal-phase Pickering emulsions in food science, Trends Food Sci. Technol. 106 (2020) 91–103.
[14] C. Albert, M. Beladjine, N. Tsapis, E. Fattal, F. Agnely, N. Huang, Pickering emulsions: preparation processes, key parameters governing their properties and potential for pharmaceutical applications, J. Control. Release 309 (2019) 302–332.
[15] Y.S. Wei, Z.C. Niu, F.Q. Wang, K. Feng, M.H. Zong, H. Wu, A novel pickering emulsion system as the carrier of tocopheryl acetate for its application in cosmetics, Mater. Sci. Eng., C 109 (2020) 110503.
[16] H. Cao, M. Escamilla, M. Anas, Z. Tan, S. Gulati, J. Yun, M.J. Green, Synthesis and electronic applications of particle-templated ti3c2t z mxene–polymer films via pickering emulsion polymerization, ACS Appl. Mater. Interfaces 13 (43) (2021) 51556–51566.
[17] Z. Bian, J. Xu, S. Zhang, X. Zhu, H. Liu, J. Hu, Interfacial growth of metal organic framework/graphite oxide composites through Pickering emulsion and their CO2 capture performance in the presence of humidity, Langmuir 31 (26) (2015) 7410–7417.
[18] S. Levine, B.D. Bowen, S.J. Partridge, Stabilization of emulsions by fine particles I. Partitioning of particles between continuous phase and oil/water interface, Colloids Surf. 38 (2) (1989) 325–343.
[19] B.P. Binks, J.H. Clint, Solid wettability from surface energy components: relevance to Pickering emulsions, Langmuir 18 (4) (2002) 1270–1273.
[20] G.J. Lee, H. Am Son, J.W. Cho, S.K. Choi, H.T. Kim, J.W. Kim, Stabilization of Pickering emulsions by generating complex colloidal layers at liquid–liquid interfaces, J. Colloid Interface Sci. 413 (2014) 100–105.
[21] B.P. Binks, S.O. Lumsdon, Stability of oil-in-water emulsions stabilised by silica particles, Phys. Chem. Chem. Phys. 1 (12) (1999) 3007–3016.
[22] B.P. Binks, A. Desforges, D.G. Duff, Synergistic stabilization of emulsions by a mixture of surface-active nanoparticles and surfactant, Langmuir 23 (3) (2007) 1098–1106.
[23] B.P. Binks, J.A. Rodrigues, W.J. Frith, Synergistic interaction in emulsions stabilized by a mixture of silica nanoparticles and cationic surfactant, Langmuir 23 (7) (2007) 3626–3636.
[24] B.P. Binks, J.A. Rodrigues, Enhanced stabilization of emulsions due to surfactant-induced nanoparticle flocculation, Langmuir 23 (14) (2007) 7436–7439.
[25] L. Liu, X. Pu, Y. Zhou, J. Zhou, D. Luo, Z. Ren, Smart Pickering water-in-oil emulsion by manipulating interactions between nanoparticles and surfactant as potential oil-based drilling fluid, Colloids Surf., A: Physicochem. Eng. Aspects 586 (2020) 124246.
[26] T.S. Horozov, B.P. Binks, T. Gottschalk-Gaudig, Effect of electrolyte in silicone oil-in-water emulsions stabilised by fumed silica particles, Phys. Chem. Chem. Phys. 9 (48) (2007) 6398–6404.
[27] H. Katepalli, V.T. John, A. Tripathi, A. Bose, Microstructure and rheology of particle stabilized emulsions: Effects of particle shape and inter-particle interactions, J. Colloid Interface Sci. 485 (2017) 11–17.
[28] C. Griffith, H. Daigle, Manipulation of Pickering emulsion rheology using hydrophilically modified silica nanoparticles in brine, J. Colloid Interface Sci. 509 (2018) 132–139.
[29] B. Derjaguin, L. Landau, The theory of stability of highly charged lyophobic sols and coalescence of highly charged particles in electrolyte solutions, Acta Physicochim. URSS 14 (633–52) (1941) 58.
[30] E.J.W. Verwey, J.T.G. Overbeek, K. Van Nes, Theory of the stability of lyophobic colloids: the interaction of sol particles having an electric double layer, Elsevier Publishing Company, 1948.
[31] D.H. Napper, Polymeric stabilization of colloidal dispersions, Vol. 3, Academic Press, 1983.
[32] A.J. Worthen, V. Tran, K.A. Cornell, T.M. Truskett, K.P. Johnston, Steric stabilization of nanoparticles with grafted low molecular weight ligands in highly concentrated brines including divalent ions, Soft Matter 12 (7) (2016) 2025–2039.
[33] C.O. Metin, J.R. Baran, Q.P. Nguyen, Adsorption of surface functionalized silica nanoparticles onto mineral surfaces and decane/water interface, J. Nanopart. Res. 14 (11) (2012) 1246.
[34] C.P. Whitby, F.E. Fischer, D. Fornasiero, J. Ralston, Shear-induced coalescence of oil-in-water Pickering emulsions, J. Colloid Interface Sci. 361 (1) (2011) 170–177.
[35] A. Saha, A. Nikova, P. Venkataraman, V.T. John, A. Bose, Oil emulsification using surface-tunable carbon black particles, ACS Appl. Mater. Interfaces 5 (8) (2013) 3094–3100.
[36] W. Song, A.R. Kovscek, Functionalization of micromodels with kaolinite for investigation of low salinity oil-recovery processes, Lab Chip 15 (16) (2015) 3314–3325.
[37] S. Varanasi, L. Henzel, L. Mendoza, R. Prathapan, W. Batchelor, R. Tabor, G. Garnier, Pickering emulsions electrostatically stabilized by cellulose nanocrystals, Front. Chem. 6 (2018) 409.
[38] W. Song, A.R. Kovscek, Spontaneous clay Pickering emulsification, Colloids Surf., A 577 (2019) 158–166.
[39] C. Griffith, H. Daigle, A comparison of the static and dynamic stability of Pickering emulsions, Colloids Surf., A 586 (2020) 124256.
[40] Y. Zhu, D.J. McClements, W. Zhou, S. Peng, L. Zhou, L. Zou, W. Liu, Influence of ionic strength and thermal pretreatment on the freeze-thaw stability of Pickering emulsion gels, Food Chem. 303 (2020) 125401.
[41] D. Hatchell, W. Song, H. Daigle, Examining the role of salinity on the dynamic stability of Pickering emulsions, J. Colloid Interface Sci. 608 (2022) 2321–2329.
[42] S.R. Raghavan, J. Hou, G.L. Baker, S.A. Khan, Colloidal interactions between particles with tethered nonpolar chains dispersed in polar media: direct correlation between dynamic rheology and interaction parameters, Langmuir 16 (3) (2000) 1066–1077.
[43] S. Takae, Y. Akiyama, H. Otsuka, T. Nakamura, Y. Nagasaki, K. Kataoka, Ligand density effect on biorecognition by PEGylated gold nanoparticles: regulated interaction of RCA120 lectin with lactose installed to the distal end of tethered PEG strands on gold surface, Biomacromolecules 6 (2) (2005) 818–824.
[44] D.R. Elias, A. Poloukhtine, V. Popik, A. Tsourkas, Effect of ligand density, receptor density, and nanoparticle size on cell targeting, Nanomed. Nanotechnol. Biol. Med. 9 (2) (2013) 194–201.
[45] E. Tran, G.L. Richmond, Interfacial Steric and Molecular Bonding Effects Contributing to the Stability of Neutrally Charged Nanoemulsions, Langmuir 37 (43) (2021) 12643–12653.
[46] B.P. Binks, S.O. Lumsdon, Pickering emulsions stabilized by monodisperse latex particles: effects of particle size, Langmuir 17 (15) (2001) 4540–4547.
[47] B.P. Binks, C.P. Whitby, Nanoparticle silica-stabilised oil-in-water emulsions: improving emulsion stability, Colloids Surf., A: Physicochem. Eng. Aspects 253 (1–3) (2005) 105–115.
[48] F. Nan, J. Wu, F. Qi, Y. Liu, T. Ngai, G. Ma, Uniform chitosan-coated alginate particles as emulsifiers for preparation of stable Pickering emulsions with stimulus dependence, Colloids Surf., A: Physicochem. Eng. Aspects 456 (2014) 246–252.
[49] J.N. Israelachvili, Intermolecular and surface forces, Academic press, 2011.
[50] C. Griffith, H. Daigle, On the shear stability of water-in-water Pickering emulsions stabilized with silica nanoparticles, J. Colloid Interface Sci. 532 (2018) 83–91.
[51] D. Hatchell, W. Song, H. Daigle, Effect of Inter-Particle Van Der Waals Attraction on the Stability of Pickering Emulsions in Brine, in: SPE Annual Technical Conference and Exhibition, OnePetro, 2021, September.
[52] G.J. Hirasaki, Wettability: fundamentals and surface forces, SPE Form. Eval. 6 (02) (1991) 217–226.
[53] J. Dong, S. Chen, D.S. Corti, E.I. Franses, Y. Zhao, H.T. Ng, E. Hanson, Effect of Triton X-100 on the stability of aqueous dispersions of copper phthalocyanine pigment nanoparticles, J. Colloid Interface Sci. 362 (1) (2011) 33–41.
[54] H. Chen, A.Z. Panagiotopoulos, Communication: Modeling electrolyte mixtures with concentration dependent dielectric permittivity, J. Chem. Phys. 148 (4) (2018) 041102.
[55] B. Vincent, J. Edwards, S. Emmett, A. Jones, Depletion flocculation in dispersions of sterically-stabilised particles ("soft spheres"), Colloids Surf. 18 (2–4) (1986) 261–281.
[56] R.M. Wiley, Limited coalescence of oil droplets in coarse oil-in-water emulsions, J. Colloid Sci. 9 (5) (1954) 427–437.
[57] K. Golemanov, S. Tcholakova, P.A. Kralchevsky, K.P. Ananthapadmanabhan, A. Lips, Latex-particle-stabilized emulsions of anti-Bancroft type, Langmuir 22 (11) (2006) 4968–4977.
[58] S. Arditty, C.P. Whitby, B.P. Binks, V. Schmitt, F. Leal-Calderon, Some general features of limited coalescence in solid-stabilized emulsions, Eur. Phys. J. E 11 (3) (2003) 273–281.

[59] R. Aveyard, J.H. Clint, T.S. Horozov, Aspects of the stabilisation of emulsions by solid particles: Effects of line tension and monolayer curvature energy, Phys. Chem. Chem. Phys. 5 (11) (2003) 2398–2409.
[60] S. Levine, B.D. Bowen, S.J. Partridge, Stabilization of emulsions by fine particles II. capillary and van der Waals forces between particles, Colloids Surf. 38 (2) (1989) 345–364.
[61] R. Aveyard, J.H. Clint, D. Nees, V.N. Paunov, Compression and structure of monolayers of charged latex particles at air/water and octane/water interfaces, Langmuir 16 (4) (2000) 1969–1979.
[62] J.T.G. Overbeek, G.J. Verhoeckx, P.L. De Bruyn, H.N.W. Lekkerkerker, On understanding microemulsions: II. Thermodynamics of droplet-type microemulsions, J. Colloid Interface Sci. 119 (2) (1987) 422–441.